

Synergistic Chaotropic Effect and Defect Engineering Promoting Ultrahigh Ionic Conductivity in MOF

Dongbo Liu^a, Xiao-Min Li^{*a}, Junchao Jia^a, Xingyu Long^a, Junpeng Yan^a, Mengyang
Xiao^a, Aziz Bakhtiyarovich Ibragimov^b, and Junkuo Gao^{*a}

a China-Uzbekistan Joint Laboratory on Advanced Porous Materials, School of
Materials Science and Engineering, Zhejiang Sci-Tech University, Hangzhou 310018,
P. R. China.

b Institute of General and Inorganic Chemistry, Uzbekistan Academy of Sciences,
Tashkent 100170, Uzbekistan

Corresponding Author: lixm@zstu.edu.cn (Xiao-Min Li); jkgao@zstu.edu.cn
(Junkuo Gao)

1. Materials and methods

1.1 Materials preparation

Chemicals: All reagents used in this study were analytical grade and without further purification. 1,4-dicarboxybenzene (H_2BDC) was obtained from Energy Chemical. $\text{ZrOCl}_2 \cdot 8\text{H}_2\text{O}$ and LiI were obtained from Macklin. Ethanol absolute ($\text{CH}_3\text{CH}_2\text{OH}$) was obtained from Gaojing Chemical Plant.

Synthesis of UiO-66 [1] : ZrCl_4 (0.24 g) and H_2BDC (0.171 g) were dissolved in 60 mL DMF. Then the obtained solution was heated in the oven at 120 °C for 48 h. After cooling to the room temperature, the solid was collected and washed with DMF and methanol each three times. Then the solid was immersed in methanol overnight. Finally, the solid product was obtained by centrifugation and dried in a vacuum oven at 80 °C overnight.

Synthesis of D-UiO-66 [2] : $\text{ZrOCl}_2 \cdot 8\text{H}_2\text{O}$ (1.5 mmol, 0.48 g) and H_2BDC (1.5 mmol, 0.25 g) were mixed and ground in a mortar by hand for about 10 min at room temperature. Then the obtained sample was transferred to a reactor and heated in an oven at 130 °C for 12h to crystallize. After cooling to room temperature, the white solid was put into the ethanol solution, stirred at 70 °C for half an hour, and then left for a while. The above processes were repeated for 3 times. Finally, the liquid was removed by centrifugation. The product was obtained by drying in a vacuum oven at 150 °C for 12h.

Synthesis of D-UiO-66-LiI: D-UiO-66 (0.55 g) and LiI (0.06 g) were mixed and ground in a mortar by hand for about 20 min, and then kept at 95% RH for 24 h.

1.2 Acid-base titration method

For D-UiO-66, there are three types of protons involved in the reaction: μ_3 -OH, -OH₂, -OH. The acid-base titration curve shows three inflection points, which may correspond to the three types of protons. The first-derivative curve is used to determine the equivalence points in the titration curve. The first point can be assigned to the μ_3 -OH proton. The other protons correspond to defect sites in the node. The second point and the third point correspond to the Zr-OH₂ proton and Zr-OH proton, respectively.

2. Ionic conductivity measurements

Firstly, the powder samples were put into a self-made mold with a radius of 0.2 cm for compression to obtain circular pellets and their thicknesses were determined by a vernier caliper. Secondly, the tablet was clipped with two pieces of gold and then the test clamp was placed on a double glass beaker container for test. Constant temperature and humidity chamber was used to control the relative humidity and temperature. The alternating current (AC) impedance data were recorded using an electrochemical workstation with a voltage of 100 mV, and the frequency range was 1 MHz ~1 Hz. The ionic conductivity (σ /S cm⁻¹) was calculated using the following equation.

$$\sigma = \frac{l}{SR}$$

where σ , l , S and R mean the conductivity (S cm⁻¹), the thickness (cm) of the pellet, the cross-sectional area (cm²) of the pellet and the bulk resistance (Ω), respectively. The activation energy (E_a) was calculated from the following equation

$$\ln\sigma_T = \ln\sigma_0 - \frac{E_a}{KT}$$

where σ , K and T mean the conductivity (S cm⁻¹), the Boltzmann constant (eV / K) and

the temperature (K), respectively. ZView software was used to get bulk resistance by fitting the semicircle of Nyquist plots. The ionic conductivity and activated energy were calculated with the above equations.

3. Device Characterizations

The powder X-ray diffraction (PXRD) measurements were performed on a Bruker D8 Advance system equipped with graphite-monochromated Cu $K\alpha$ radiation ($\lambda = 1.5418 \text{ \AA}$). The acquisition parameters comprised a continuous scan mode with an angular velocity of $5^\circ \cdot \text{min}^{-1}$ over the 2θ interval of $5\text{-}50^\circ$. Thermogravimetric profiles were obtained via a NETZSCH TG 209 F1 thermal analyzer by linearly heating specimens from 25°C to 900°C at $10^\circ\text{C} \cdot \text{min}^{-1}$ under a nitrogen-purged environment. Specific surface area determinations were executed through low-temperature (77 K) nitrogen sorption experiments, with subsequent Brunauer-Emmett-Teller (BET) model fitting to the adsorption branch data. The Fourier transform infrared (FT-IR) data were collected by a Fourier transform infrared spectrometer (Nicolet 5700, Thermo Electron Corp., USA) in the range of $4000\text{-}400 \text{ cm}^{-1}$. Temperature-dependent FT-IR spectrum tests used ATR (attenuated total reflectance) attachment. The ^7Li VT-SSNMR spectra were performed by a Bruker 1272 instrument.

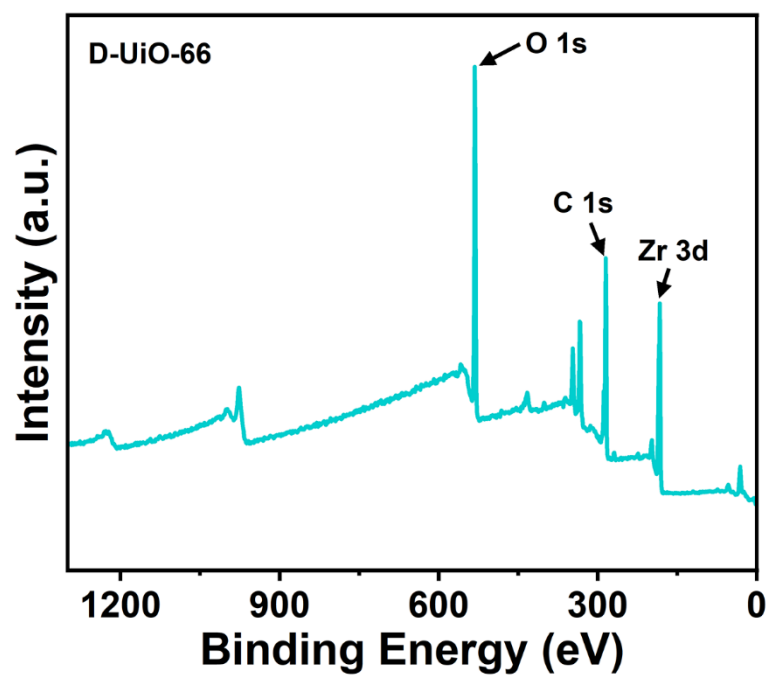


Fig. S1. XPS spectrum of D-UiO-66.

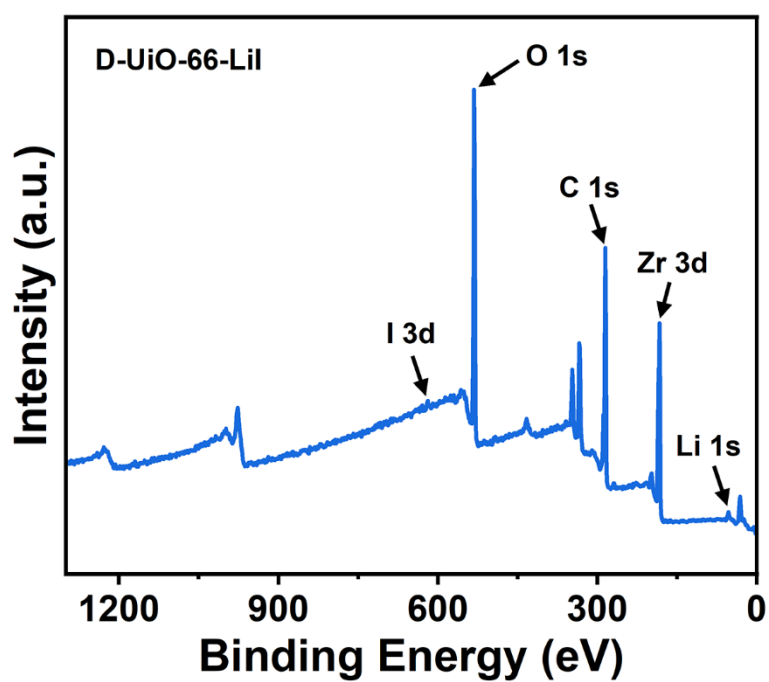


Fig. S2. XPS spectrum of D-UiO-66-LiI.

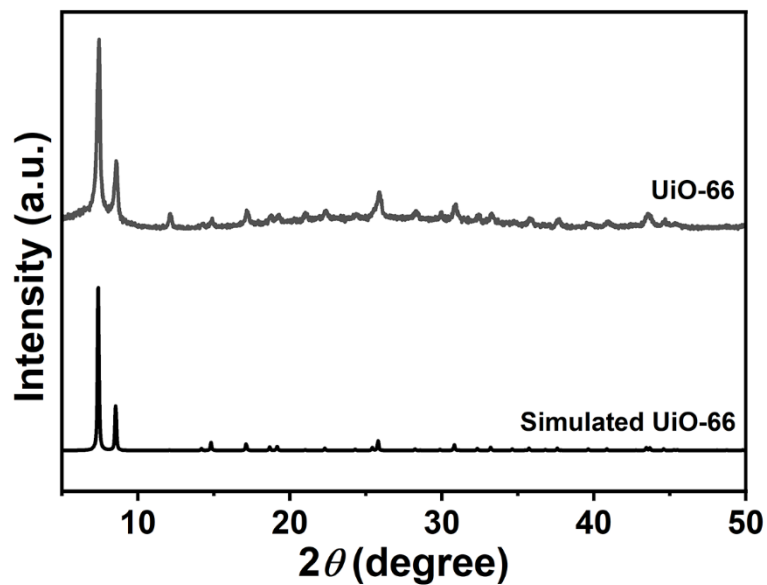


Fig. S3. PXRD patterns of simulated UiO-66 and as-synthesized UiO-66.

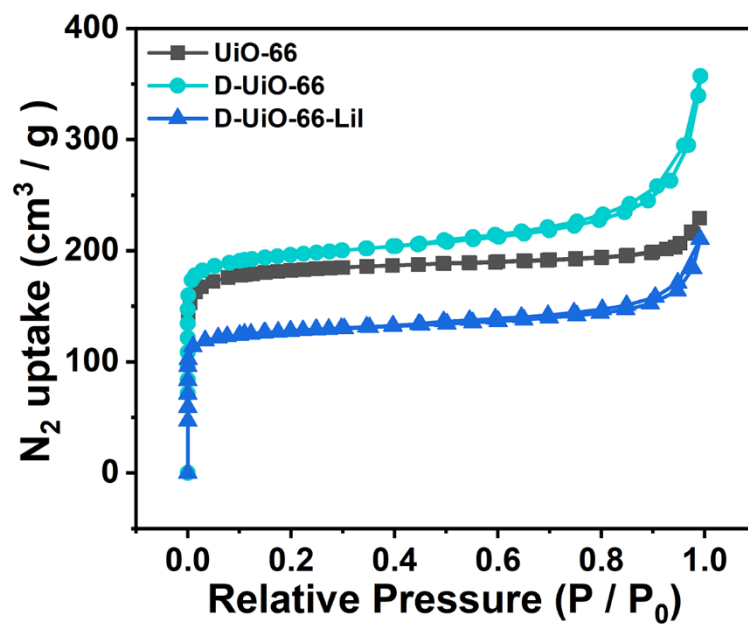


Fig. S4. N_2 adsorption-desorption isotherms of UiO-66, D-UiO-66, and D-UiO-66-LiI.

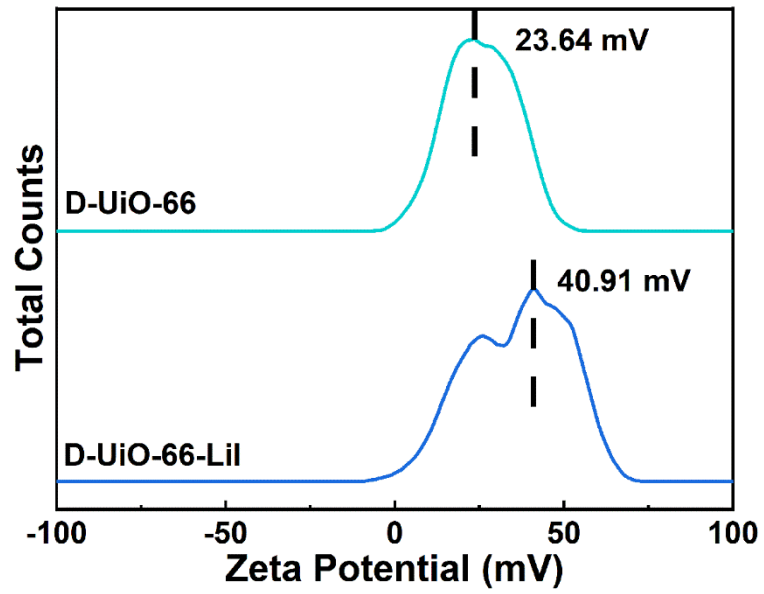


Fig. S5. Zeta potential of D-UiO-66 and D-UiO-66-LiI.

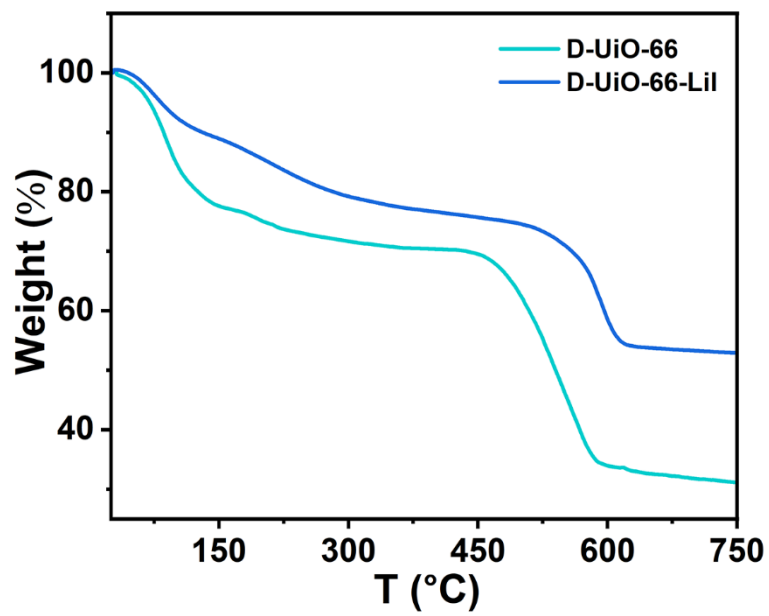


Fig. S6. TGA curves of D-UiO-66 and D-UiO-66-LiI.

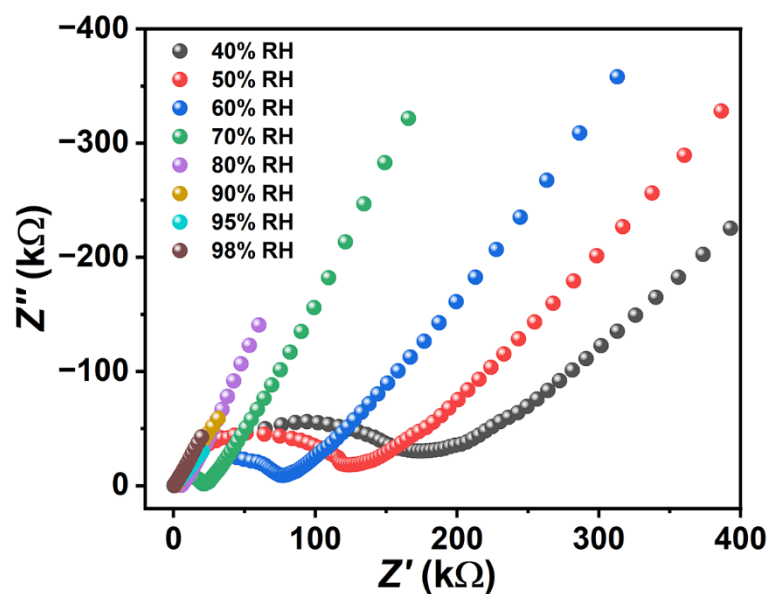


Fig. S7. Nyquist plots of D-UiO-66 at 30 °C and different humidities variation from 40% to 98% RH.

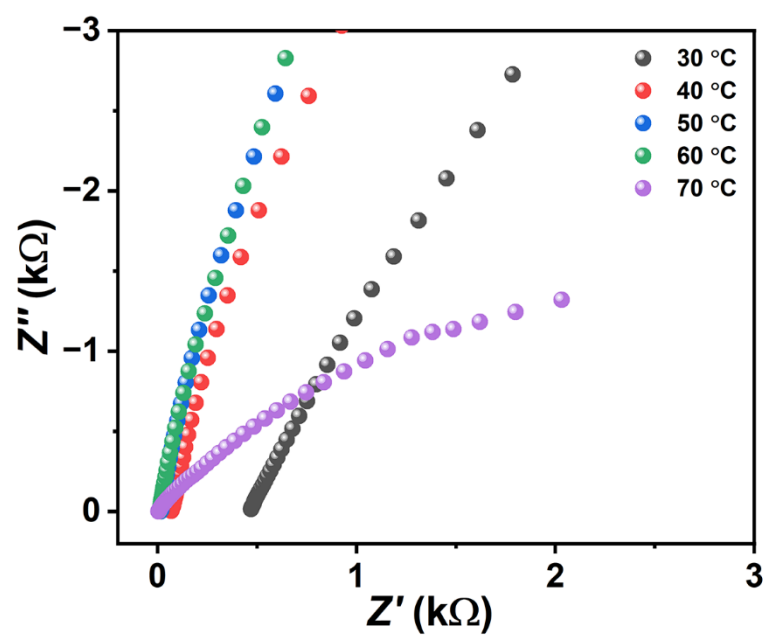


Fig. S8. Nyquist plots of D-UiO-66 at 98% RH and different temperatures variation from 30 to 70 °C.

Table S1. The comparison of D-UiO-66-LiI with some other representative MOFs-

based ion conducting materials.

Material	Ionic Conductivity (S cm ⁻¹)	Condition	Activation Energy (eV)	Reference
D-UiO-66-LiI	5.03×10^{-1}	70 °C, 98% RH	0.48	This work
MIL53(Al)@LiCoD	1.8×10^{-3}	100 °C, 75% RH	/	3
Ti-dobdc-LiI	1.88×10^{-2}	25 °C, 90% RH	<0.4	4
Mg ₂ (dobdc)·0.35LiO ⁱ Pr·0.25LiBF ₄ ·EC·DEC	3.1×10^{-4}	27 °C	0.15	5
LiOtBu-grafted UiO-66	1.8×10^{-5}	25 °C	0.18	6
PEO-MIL-53(Al)-LiTFSI	3.39×10^{-3}	120 °C	/	7
MOF-LiI	1.1×10^{-4}	25 °C	0.24	8
EMI-TFSA@ZIF-8	2.6×10^{-5}	22 °C	0.35	9
EMIMCl@UiO-67	1.67×10^{-3}	200 °C	0.37	10
SA-EIMS@MIL-101	1.89×10^{-3}	150 °C	0.26	11

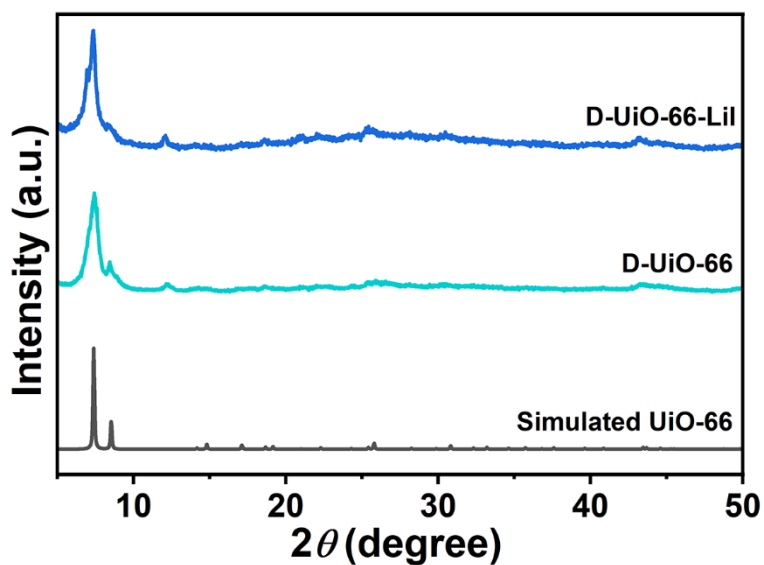


Fig. S9. PXRD patterns of simulated UiO-66, D-UiO-66 after ion conduction measurements, and **D-UiO-66-LiI** after ion conduction measurements.

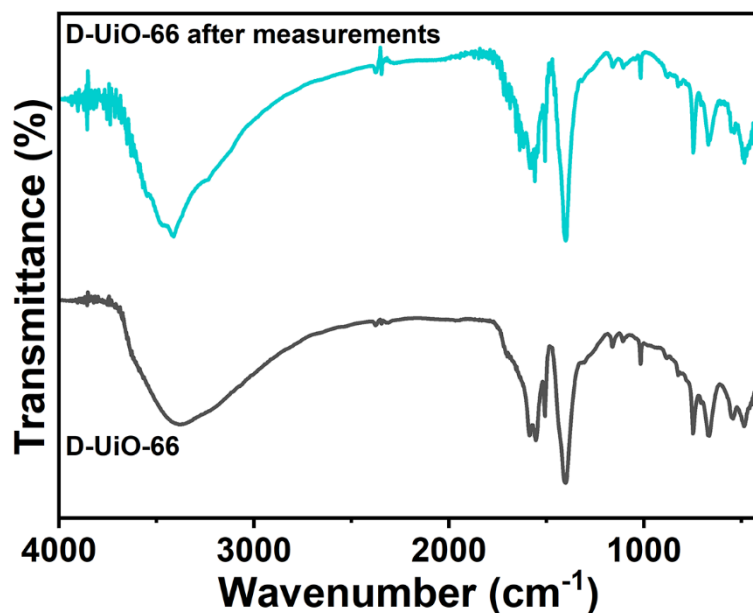


Fig. S10. FT-IR spectra of as-synthesized D-UiO-66 and D-UiO-66 after ion conduction measurements.

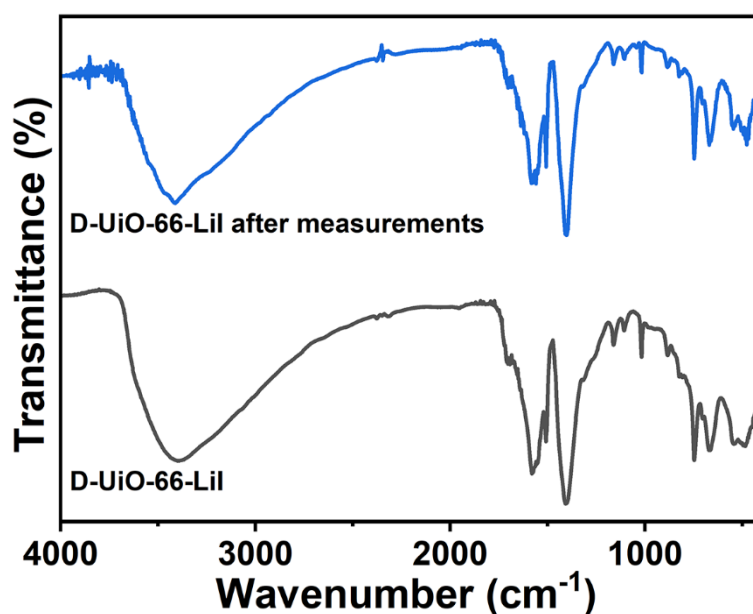


Fig. S11. FT-IR spectra of as-synthesized **D-UiO-66-LiI** and **D-UiO-66-LiI** after ion conduction measurements.

conduction measurements.

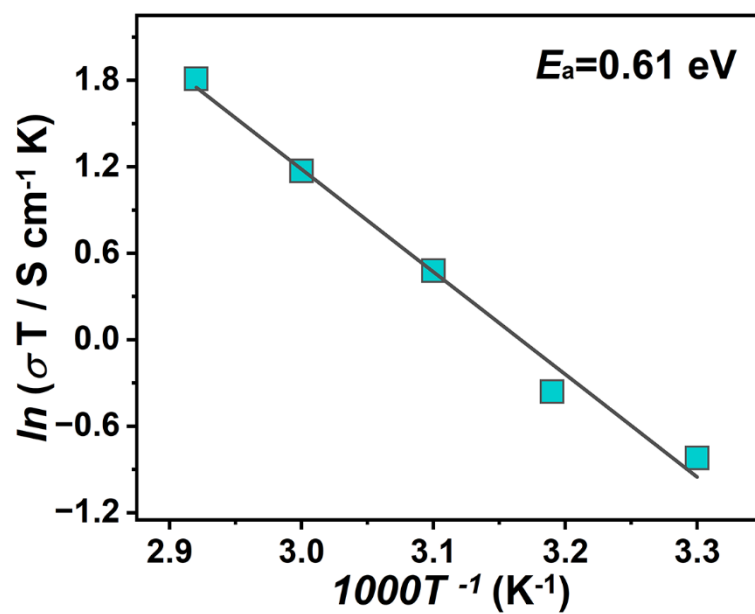


Fig. S12. Arrhenius plot of D-UiO-66 at 98% RH and in the temperature range of 30-70 °C.

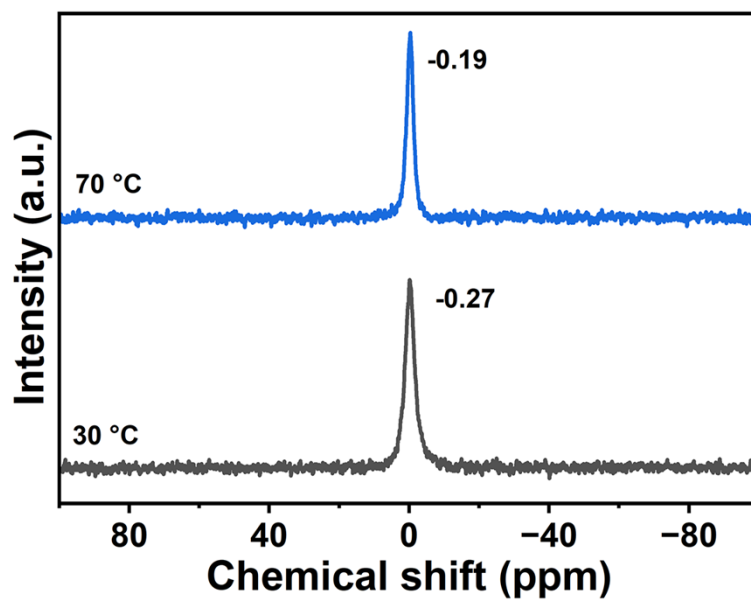


Fig. S13. ^7Li VT-SSNMR spectra of D-UiO-66-LiI at 30 °C and 70 °C.

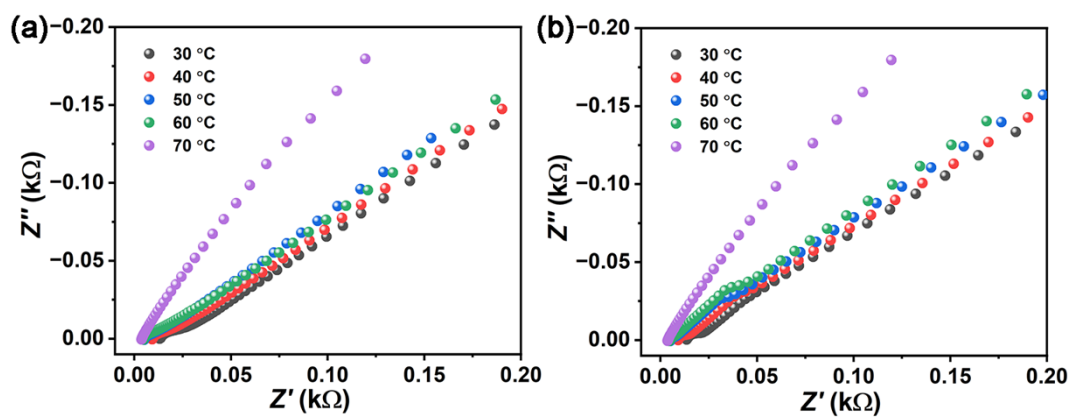


Fig. S14. Nyquist plot for the heating-cooling cycle of **D-UiO-66-LiI** at 98% RH: (a) the heating cycle (30-70 °C); (b) the cooling cycle (70-30 °C).

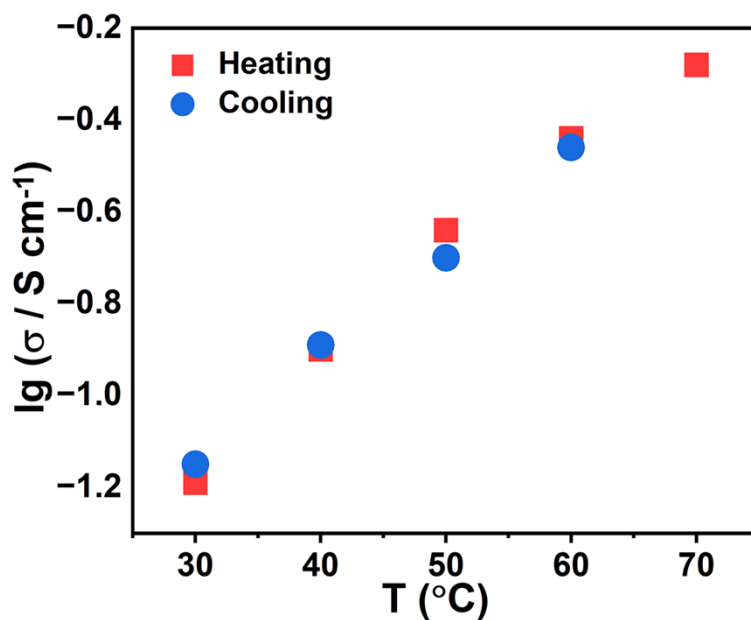


Fig. S15. Ionic conductivities for the heating-cooling cycle of **D-UiO-66-LiI** at 98% RH.

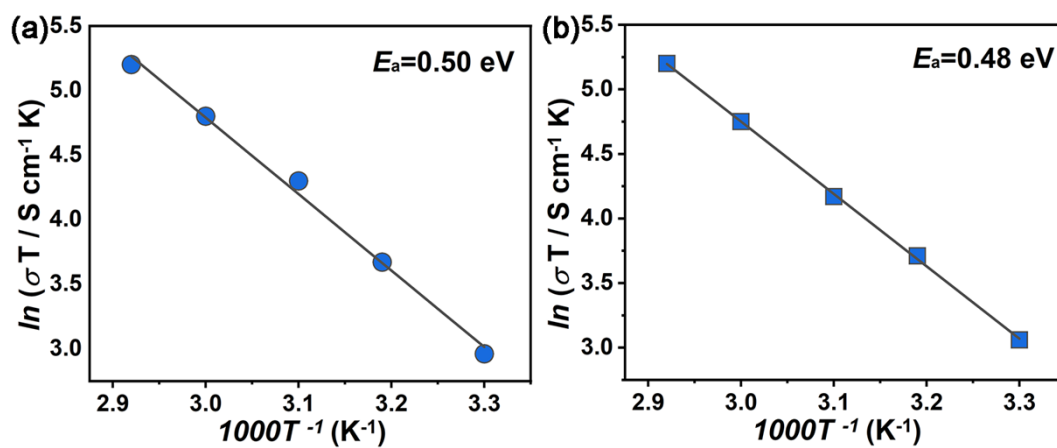


Fig. S16. Arrhenius plots of **D-UiO-66-LiI** for every heating-cooling cycle at the temperature range of 30-70 °C and 98% RH: (a) the heating cycle (30-70 °C); (b) the cooling cycle (70-30 °C).

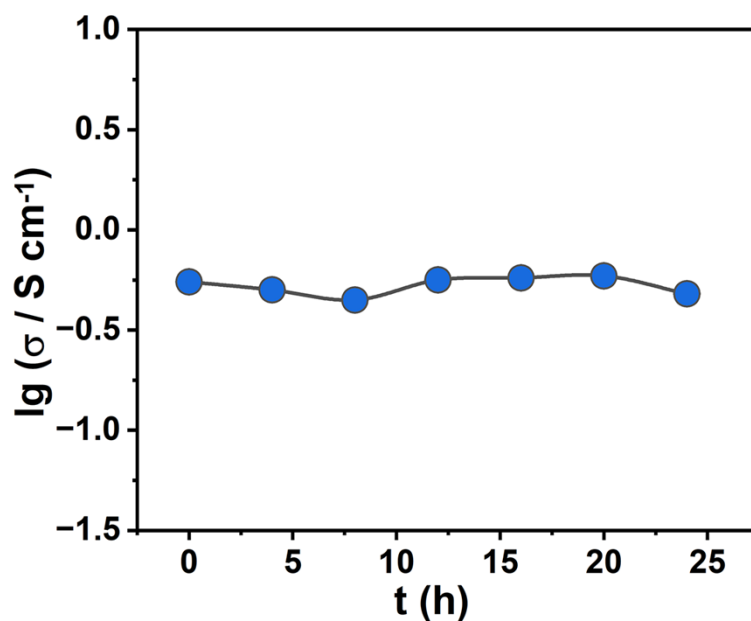


Fig. S17. The time-dependent ionic conductivities of **D-UiO-66-LiI** measured at 70 °C and 98% RH.

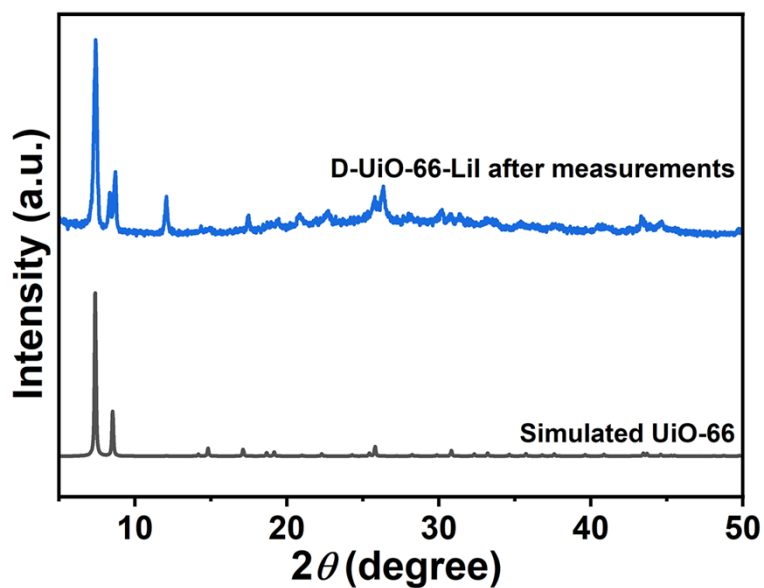


Fig. S18. PXRD patterns of as-synthesized **D-UiO-66-LiI** and **D-UiO-66-LiI** after temperature cycling and time-dependent ion conduction measurements.

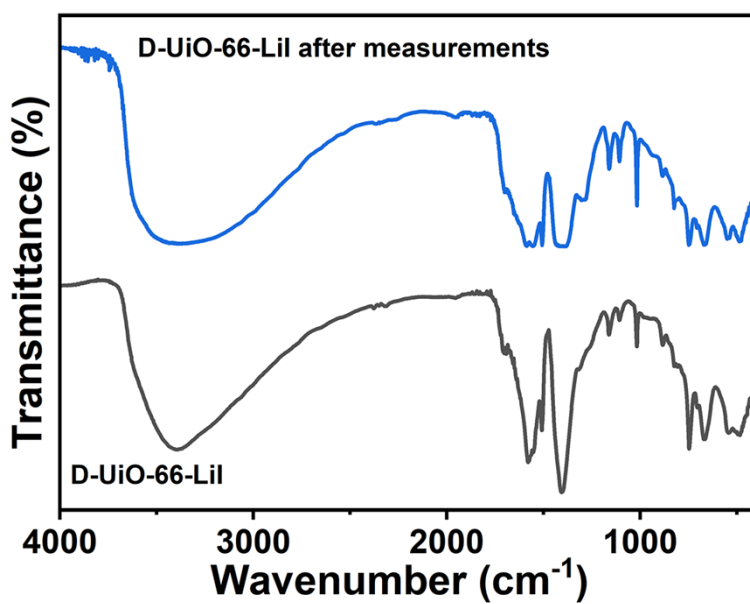


Fig. S19. FT-IR spectra of as-synthesized **D-UiO-66-LiI** and **D-UiO-66-LiI** after temperature cycling and time-dependent ion conduction measurements.

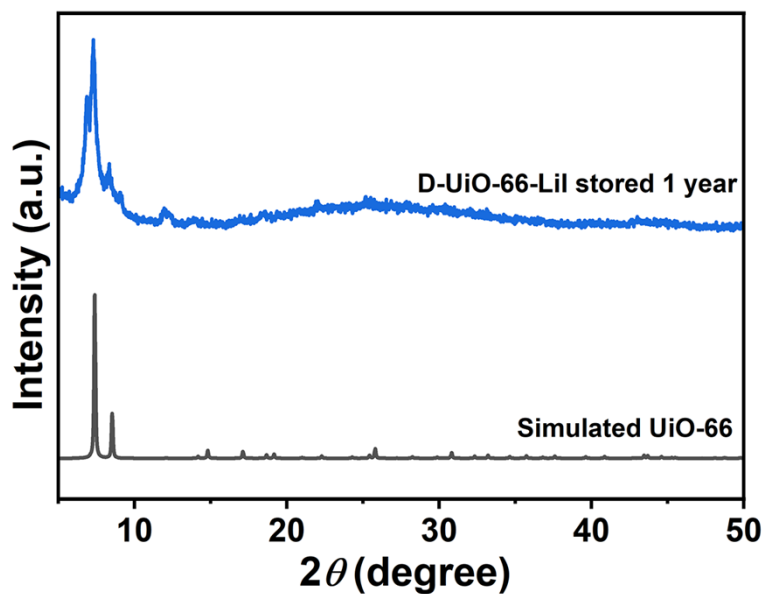


Fig. S20. The PXRD patterns of simulated UiO-66 and **D-UiO-66-LiI** stored for 1 year.

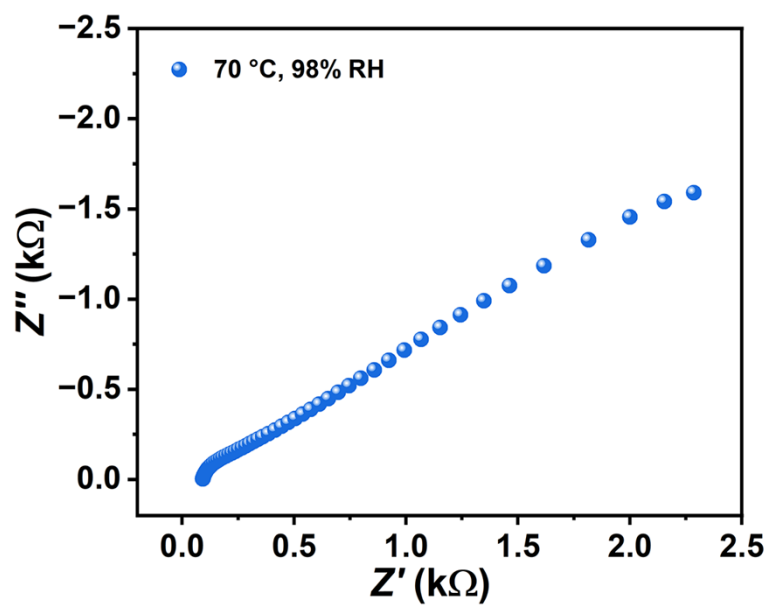


Fig. S21. Nyquist plot of **D-UiO-66-LiI** stored for 1 year at 70 °C and 98% RH.

References

- [1] J. H. Cavka, S. Jakobsen, U. Olsbye, N. Guillou, C. Lamberti, S. Bordiga and K. P. Lillerud, *J. Am. Chem. Soc.*, 2008, **130**, 13850-13851.

- [2] G. Ye, D. Zhang, X. Li, K. Leng, W. Zhang, J. Ma, Y. Sun, W. Xu and S. Ma, *ACS Appl. Mater. Interfaces*, 2017, **9**, 34937-34943.
- [3] J. Brus, J. Czernek, M. Urbanova, J. Rohlíček and T. Plecháček, *ACS Appl. Mater. Interfaces*, 2020, **12**, 47447-47456.
- [4] M. K. Sarango-Ramírez, M. Donoshita, Y. Yoshida, D.-W. Lim and H. Kitagawa, *Angew. Chem. Int. Ed.*, 2023, **62**, e202301284.
- [5] B. M. Wiers, M.-L. Foo, N. P. Balsara and J. R. Long, *J. Am. Chem. Soc.*, 2011, **133**, 14522-14525.
- [6] R. Ameloot, M. Aubrey, B. M. Wiers, A. P. Gómora-Figueroa, S. N. Patel, N. P. Balsara and J. R. Long, *Chem. Eur. J.*, 2013, **19**, 5533-5536.
- [7] K. Zhu, Y. Liu and J. Liu, *RSC Adv.*, 2014, **4**, 42278-42284.
- [8] E. M. Miner, S. S. Park and M. Dincă, *J. Am. Chem. Soc.*, 2019, **141**, 4422-4427.
- [9] K. Fujie, K. Otsubo, R. Ikeda, T. Yamada and H. Kitagawa, *Chem. Sci.*, 2015, **6**, 4306-4310.
- [10] L.-H. Chen, B.-B. Wu, H.-X. Zhao, L.-S. Long and L.-S. Zheng, *Inorg. Chem. Commun.*, 2017, **81**, 1-4.
- [11] H. Chen, S.-Y. Han, R.-H. Liu, T.-F. Chen, K.-L. Bi, J.-B. Liang, Y.-H. Deng and C.-Q. Wan, *J. Power Sources*, 2018, **376**, 168-176.